Collapse of the coherence gap in Kondo semiconductors

Peter S. Riseborough
Department of Physics, Temple University, Barton Hall, 1900 North 13th Street, Philadelphia, Pennsylvania 19122, USA
(Received 13 March 2003; revised manuscript received 11 July 2003; published 31 December 2003)

Kondo semiconductors exhibit a gap in their low-temperature excitation spectra, and can be modeled by the Anderson lattice model at half filling which shows a hybridization gap. The mixed-valent Kondo semiconductor SmB_6 also shows in-gap magnetic excitations that exhibit the temperature dependence and dispersion that are expected from magnetic excitons. The gaps measured in the Kondo semiconductors are extremely sensitive to doping in which the f ions are substituted by non-f ions. Recent measurements on YbB_{12} shows a feature similar to that of the magnetic exciton in SmB_6. Furthermore, the concentration dependence of the features observed in inelastic neutron-scattering spectra of doped YbB_{12} is different from the concentration dependence found in measurements of thermodynamic and transport properties. The impurity concentration dependence of the gap and the spin-exciton features are investigated. The spectroscopic properties are calculated for the Anderson lattice model at half filling, in which the disorder is treated in the coherent potential approximation. The results are compared with the recent experiments.

DOI: 10.1103/PhysRevB.68.235213 PACS number(s): 75.30.Mb, 71.27.+a

I. INTRODUCTION

The low-temperature thermodynamic, transport, and spectroscopic properties of Kondo semiconductors, or heavy fermion semiconductors[1,2] such as $Ce_3Bi_4Pt_4$ (Ref. 3), SmB_6 (Ref. 4), or YbB_{12} (Ref. 5) are dominated by extremely small temperature-dependent gaps of the order of tens of degrees Kelvin. In contrast to ordinary semiconductors, the extremely small magnitude of the low-temperature gap is attributed to renormalization caused by the strong electron-electron interactions between the electrons in the f shell. Gaps have been observed in inelastic neutron-scattering[6–9] and optical-absorption[10–13] measurements at sufficiently low-temperatures. Inelastic neutron-scattering experiments on the low-temperature state of strongly mixed-valent material SmB_6 (Ref. 7) show the existence of sharp branch of dispersive magnetic excitations within the gap. Similar features were also found in polycrystalline samples of YbB_{12}.[8,9] At temperatures higher than the gap energy, the thermal population of electron-hole pairs participate in quasielastic scattering. This results in that the gaps observed in optical-absorption[10–13] and inelastic neutron-scattering spectra[6–9] vanish. In this high-temperature regime, the properties of the Kondo semiconductors resemble those of a heavy-fermion or mixed-valent materials.

Compounds such as CeNiSn (Ref. 14), CeRhSb (Ref. 15), and FeSi (Ref. 16) are materials that are closely related to the Kondo semiconductors. Careful studies of high quality crystals of CeNiSn (Ref. 17) have revealed that although the compound does have a pseudogap structure in the quasiparticle density of states, the material is very anisotropic and metallic.[17] Recently, the T^2 term in the low-temperature resistivity of CeNiSn has been found to have a large coefficient, and Shubnikov–de Haas oscillations have been measured.[18] These recent observations confirm that CeNiSn is a semimetal. The appropriateness of describing the transition-metal compound FeSi as a Kondo semiconductor has also been called into question,[19–21] since the d band has a width which is comparable to the width of the gap and, therefore, the simple Kondo picture used in this work might not apply.

The properties of the Kondo semiconductors are reasonably well described by those of the Anderson lattice model in which the semiconducting state occurs when the hybridization gap straddles the Fermi energy.[22,23] The hybridization gap is subject to many-body renormalizations that produce a temperature-dependent reduction of its magnitude which is consistent with the behavior of the gap determined experimentally from transport measurements.[24] The behavior of the gap has been investigated in a series of experiments in which the f ions have been substituted with non-f ions.[3,25–27] Substitutional doping has the effect of collapsing the gap structure in the density of states. The hybridization gap is a direct manifestation of the coherence of the f ions, and the introduction of substitutional disorder has been shown to produce impurity states within the gap.[28,29] The theoretical description[28–31] is quite consistent with the experimentally observed specific heat and resistivity. Thus, for example, the existence of impurity states roughly 3 meV below the upper edge of the hybridization gap quite naturally explains resistivity[32,33] and tunneling measurements[34] on SmB_6, while optical[11] and point-contact spectroscopy[35] indicate that the magnitude of the overall hybridization gap is of the order of 20 meV.

The sharp dispersive mode within the gap found in the magnetic response of SmB_6 (Ref. 7) has the same dispersion relation and temperature dependence as predicted for spin-exciton excitations.[36] Spin-exciton excitations can be envisaged as bound states of electron-hole pair excitations caused by the strong antiferromagnetic exchange. Alternatively, the spin-exciton excitations can be thought of as continuations of the antiferromagnetic paramagnonlike excitations which occur at energies above the threshold of the continua of electron-hole pairs. The antiparamagnon excitations usually only exist as a resonance within the continua of spin-flip electron-hole pair (Stoner) excitations which, for metals, extend down to zero energy. Therefore, to a first approximation, antiparamagnons should only exist above the gap in a

semiconductor. However, in the Kondo insulators which have large strengths of the antiferromagnetic interactions, these branches of excitations soften at low-temperatures and continue within the hybridization gap, thereby forming the branches of spin-exciton excitations. Since the widths of the antiparamagnon resonances are caused by an electron-hole pair decay channel, the broad antiparamagnon peaks undergo significant narrowing at energies below the threshold of the Stoner excitations.

While analysis of transport measurements[5] of YbB_{12} yields an activation energy of 10 meV, presumably dominated by the pinning of the Fermi level to impurities, the optical absorption measurements[13] indicate that the magnitude of the intrinsic gap is about 20 meV. Earlier inelastic neutron scattering measurements on YbB_{12} (Refs. 8 and 9) showed the existence of magnetic scattering peaks around 15 and 20 meV. The temperature dependence of the 15 meV peak is indicative of it having a many-body origin, perhaps being a spin-exciton excitation. The results of recent inelastic neutron-scattering experiments[37] on YbB_{12} have been claimed to indicate a difference in the concentration dependence of the gap from that observed in thermodynamic properties. Since YbB_{12} may also support spin-exciton excitations, this discrepancy might be due to the spin-exciton having a different sensitivity to impurities. In this paper, we shall examine the effects of disorder on the dynamic magnetic response, particularly focusing on the branch of spin-exciton excitations. The heavy-fermion semiconductors will be modeled by the Anderson lattice model. The effect of the impurities is treated within the coherent potential approximation (CPA). We shall compare our results with the measured inelastic neutron scattering and the thermodynamic properties of the mixed-valent Kondo semiconductors.

II. DISORDERED ANDERSON LATTICE MODEL

The heavy-fermion semiconductors are modeled by the Anderson lattice model at half filling. The Hamiltonian is written as the sum of three terms:

$$\hat{H}=\hat{H}_f+\hat{H}_d+\hat{H}_{fd}. \tag{1}$$

The first term $\hat{H}_f$ describes the Hamiltonian of the degenerate localized f electronic states. It is written as

$$\hat{H}_f=\sum_{j,\alpha} E_{f,j} f^{\dagger}_{j,\alpha} f_{j,\alpha}+\sum_{j,\alpha,\beta}\frac{U_{ff}}{2} f^{\dagger}_{j,\alpha} f^{\dagger}_{j,\beta} f_{j,\beta} f_{j,\alpha}, \tag{2}$$

where the index α labels the states of the N_f-fold degenerate f level while $f^{\dagger}_{j,\alpha}$ and $f_{j,\alpha}$, respectively, are the creation and annihilation operators for an f electron with degeneracy index α at site j. The term proportional to $E_{f,j}$ represents the binding energy of a single f electron at site j and the term proportional to U_{ff} describes the Coulomb repulsion between a pair of electrons located on the same lattice site. The term $\hat{H}_d$ is the Hamiltonian of the conduction electron states. It is written as

$$\hat{H}_d=\sum_{\underline{k},\alpha} \epsilon(\underline{k}) d^{\dagger}_{\underline{k},\alpha} d_{\underline{k},\alpha}, \tag{3}$$

where $d^{\dagger}_{\underline{k},\alpha}$ and $d_{\underline{k},\alpha}$ are, respectively, the creation and annihilation operators for a conduction electron with the degeneracy index α in the Bloch state labeled by the wave vector $\underline{k}$. Since all the known Kondo semiconductors have cubic symmetry,[1] the dispersion relation $\epsilon(\underline{k})$ for the conduction electrons is calculated in the tight-binding approximation for a simple cubic lattice, with hopping matrix element t. The bandwidth is denoted by W and is given by $W=12t$. The term $\hat{H}_{fd}$ represents the hybridization which couples the localized f levels and the itinerant conduction band states. The hybridization interaction $\hat{H}_{fd}$ is written as

$$\hat{H}_{fd}=\frac{1}{\sqrt{N}}\sum_{\underline{k},j,\alpha}\{V\exp[+i\underline{k}.\underline{R}_j] d^{\dagger}_{\underline{k},\alpha} f_{j,\alpha} + V^{*}\exp[-i\underline{k}.\underline{R}_j] f^{\dagger}_{j,\alpha} d_{\underline{k},\alpha}\}. \tag{4}$$

The first term represents the process in which an electron with quantum number α tunnels out of the f orbital on site j into the conduction-band state labeled by Bloch wave vector $\underline{k}$. The second term is the Hermitian conjugate and represents the reverse process. The quantum number α is conserved in the tunneling process and the matrix element V represents the strength of the isotropic hybridization. Ikeda and Miyake[38] have proposed that CeNiSn can be described by a similar hybridization gap model, in which the hybridization is highly anisotropic and vanishes for certain directions in the Brillouin zone. The vanishing of the gap along these directions leads to a semimetallic state. A competing theoretical picture of CeNiSn starts by assuming a spin charge separated state.[39]

Since the Coulomb repulsion U_{ff} is the largest energy scale in the problem, we shall take the limit $U_{ff}\rightarrow\infty$. This limit precludes multiple occupation of the f orbitals at any site. The f electron operators are replaced by the product of f quasiparticle operators and slave boson operators. In the $U_{ff}\rightarrow\infty$ limit, the Coulomb interaction is treated by enforcing a constraint on the f quasiparticle and boson operators. In the mean-field approximation, which is exact in the limit of large degeneracy $N_f\rightarrow\infty$, the slave boson amplitude is replaced by a complex number. Thus, the Coulomb repulsion produces renormalized quasiparticle bands. The Coulomb repulsion renormalizes the position of the f level, E_f to a new position $\tilde{E}_f$ just above the chemical potential μ, and also reduces the hybridization strength from V to $\tilde{V}$. These renormalizations are expressed[22] as

$$E_f\rightarrow\tilde{E}_f=E_f+\lambda,$$

$$V\rightarrow\tilde{V}=V\sqrt{1-n_f(T)}, \tag{5}$$

where $n_f(T)$ is the temperature-dependent average number of f electrons per unit cell, and the f energy shift λ is determined by a self-consistency condition. The self-consistency conditions are evaluated as

$$\lambda[1-n_f(T)]=\frac{1}{N}\sum_{\underline{k},\alpha}\int_{-\infty}^{\infty}\frac{d\omega}{\pi}f(\omega)\tilde{V}^{*}\mathrm{Im}\,G^{df}(\underline{k},\underline{k};\omega+i\delta), \tag{6}$$

where the off-diagonal Green's function $G^{df}(k,k';\omega)$ is given in terms of the f quasiparticle Green's function $G^{ff}(\underline{k},\underline{k}';\omega)$ via

$$G^{df}(\underline{k},\underline{k}';\omega)=\frac{\tilde{V}}{[\omega-\epsilon(\underline{k})]}G^{ff}(\underline{k},\underline{k}';\omega) \tag{7}$$

and the number of f electrons per unit cell is given by

$$n_f(T)=-\frac{1}{N}\sum_{\underline{k},\alpha}\int_{-\infty}^{\infty}\frac{d\omega}{\pi}f(\omega)\mathrm{Im}G^{ff}(\underline{k},\underline{k};\omega+i\delta). \tag{8}$$

The f quasiparticle Green's function of the homogeneous system is evaluated as

$$G^{ff}(\underline{k},\underline{k}';\omega)=\delta^3(\underline{k}-\underline{k}')\frac{[\omega-\epsilon(\underline{k})]}{(\omega-\tilde{E}_f)[\omega-\epsilon(\underline{k})]-|\tilde{V}|^2}. \tag{9}$$

The upward renormalization of E_f has the effect of reducing the number of f electrons, n_f, and, therefore, minimizes the effect of the Coulomb repulsion. The renormalization of the hybridization matrix element represents the average reduction in the probability that a quasiparticle will tunnel from the conduction band into an f level, as the Coulomb interaction forbids tunneling into a level that is already occupied. The conduction bands and the f quasiparticle bands hybridize and form bands with mixed character. The bands are separated by an indirect gap of magnitude $\sim 4\tilde{V}^2/W$ in an energy range centered on $\tilde{E}_f$. The magnitude of the direct gap is given by $2\tilde{V}$. In the Kondo semiconductors, the lower hybridized bands are completely filled, and the upper hybridized bands are completely unoccupied. The f character in the quasiparticle bands has an integrated intensity which is reduced by a factor of $(1-n_f)$. The remainder of the integrated intensity shows up as an incoherent excitation located at the position of the bare f level E_f,[40] and can be measured in photoemission measurements. The many-body effects will be calculated for the stoichiometric system, and the effects of the small impurity concentrations on the many-body renormalizations will be neglected.

We shall denote the various configurations of the impurities by the index γ. We shall assume that the impurities are randomly distributed so that the different sites are independent. Thus, the probability of a particular configuration, P_γ, is the product of the probabilities for the various sites, $p_{j,\gamma}$,

$$P_\gamma=\prod_j p_{j,\gamma}. \tag{10}$$

A lattice site j has a probability that the site is occupied by a non-f ion which is given by the concentration $p_{j,2}=c$, and the probability that the site is occupied by an f ion is given by $p_{j,1}=(1-c)$. When a non-f impurity ion is located at site j, the f level binding energy $E_{f,j}$ at that site is moved above the Fermi energy, leading to the f orbital being unoccupied. The binding energy at the site j is given by

$$E_{f,j}=E_f+\Delta E_f \tag{11}$$

when an impurity is present, $\alpha=2$, and as

$$E_{f,j}=E_f \tag{12}$$

when an f ion is located at the site $\alpha=1$. We shall take the limit $\Delta E_f\rightarrow\infty$ which corresponds to the case of La impurities in $Ce_3Bi_4Pt_3$ or Lu impurities in the electron-hole analog YbB_{12}. When this limit is taken, the effect of the Coulomb shift on ΔE_f can be safely neglected.

III. COHERENT POTENTIAL APPROXIMATION

The effect of disorder is treated within the single-site approximation using the CPA In the CPA, the local Green's function $G^{ff}_{jj}(\omega)$ is replaced by the configurational averaged local Green's function $\tilde{G}^{ff}(\omega)$, which describes the effective medium. The configurational averaged local Green's function has periodic translation symmetry and, therefore, is independent of the site index j. As a consequence, the Fourier components of the configurational averaged Green's functions are diagonal in the Bloch wave vector $\underline{k}$. Thus, the configurational averaged Green's function can be written in the same form as that of the ordered system, but in which a complex self-energy $\Sigma(\omega)$ is introduced to replace the renormalized f level binding energy $\tilde{E}_f$. Thus,

$$\begin{aligned}\tilde{G}^{ff}(\omega)&=\sum_\gamma P_\gamma G^{ff}_{jj}(\omega)\\&=\sum_\gamma P_\gamma\frac{1}{N}\sum_{\underline{k},\underline{k}'}G^{ff}(\underline{k},\underline{k}';\omega)\delta^3(\underline{k}-\underline{k}')\\&=\frac{1}{N}\sum_{\underline{k}}\tilde{G}^{ff}(\underline{k},\underline{k};\omega)\\&=\frac{1}{N}\sum_{\underline{k}}\frac{[\omega-\epsilon(\underline{k})]}{[\omega-\Sigma(\omega)][\omega-\epsilon(\underline{k})]-|\tilde{V}|^2}.\end{aligned} \tag{13}$$

In the CPA,[41–43] the complex self-energy is determined by the condition that the configurational averaged T matrix for the entire solid vanishes. This leads to the condition that the single-site T matrix also vanishes:

$$T_j(\omega)=\sum_\gamma\frac{p_{j,\gamma}[\tilde{E}_{f,j}-\Sigma(\omega)]}{1-[\tilde{E}_{f,j}-\Sigma(\omega)]\tilde{G}^{ff}(\omega)}=0. \tag{14}$$

This condition is simply evaluated as

$$\tilde{G}^{ff}(\omega)=\frac{c}{[\tilde{E}_f-\Sigma(\omega)]}+\frac{(1-c)}{[\tilde{E}_f+\Delta E_f-\Sigma(\omega)]}, \tag{15}$$

where the, site diagonal, f quasiparticle Green's function is given by

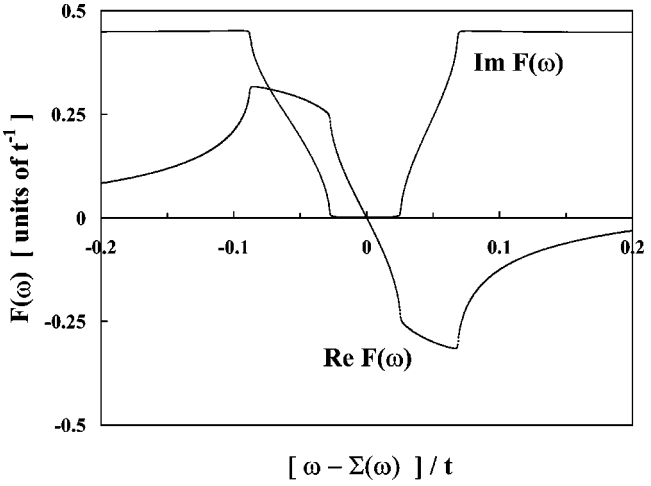

FIG. 1. The ω dependence of the real and imaginary parts of the function $F(\omega)$, defined in the text by Eq. (17), for fixed Σ. The renormalized parameters are given by $\tilde{V}=0.4t$ and $\tilde{E}_f=0.266\,66t$. The imaginary part of F is marked by the solid line. In general, the imaginary part of $F(\omega)$ is zero in the frequency range outside the band width $|\omega|>6t$ and inside the hybridization gap $|\tilde{V}^2|>\omega 6t$. The real part of $F(\omega)$ is marked by the dotted line. It shows a rapid variation near the edges of the hybridization gap.

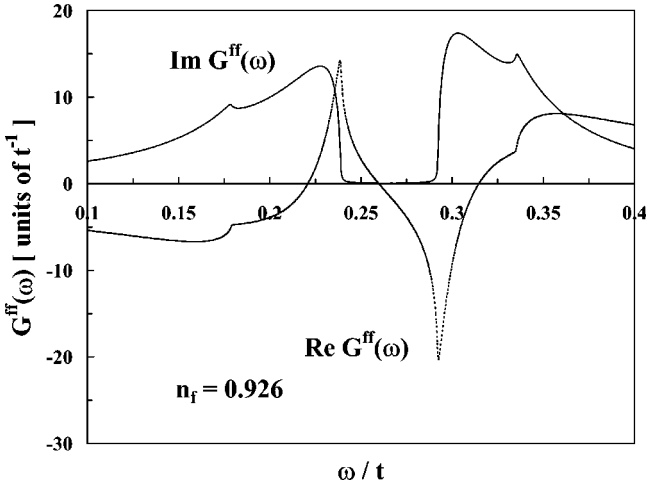

FIG. 2. The real and imaginary parts of the local f Green's function $G^{ff}(\omega)$, defined by Eq. (13), for the undoped system [$c=0$, $\Sigma(\omega)=\tilde{E}_f$]. The real part is shown by the dotted line and the imaginary part is marked by a solid line. The values of the parameters used are the same as in Fig. 1. The imaginary part of the f Green's function is zero inside the hybridization gap, but peaks up close to the gap edges. The real part of the f Green's function varies rapidly close to the gap edges.

$$\tilde{G}^{ff}(\omega)=\frac{1}{[\omega-\Sigma(\omega)]}\left[1+\frac{|\tilde{V}|^2}{[\omega-\Sigma(\omega)]}F(\omega)\right] \tag{16}$$

and

$$F(\omega)=\frac{1}{N}\sum_{\underline{k}}\left[\omega-\epsilon(\underline{k})-\frac{|\tilde{V}|^2}{\omega-\Sigma(\omega)}\right]^{-1}. \tag{17}$$

The real and imaginary parts of $F(\omega+i\delta)$, for a fixed real value of Σ, are plotted in Fig. 1. It should be noticed that the imaginary part of F vanishes for values of ω near Σ due to the presence of the hybridization gap. Also the real part of the function is approximately linear in this range of ω. In fact, for $\omega\sim\Sigma$, the function has the asymptotic expansion:

$$F(\omega)=-\frac{(\omega-\Sigma)}{|\tilde{V}|^2}\left[1+\omega\frac{(\omega-\Sigma)}{|\tilde{V}|^2}+\left(\frac{W^2}{24}+\omega^2\right)\frac{(\omega-\Sigma)^2}{|\tilde{V}|^4}+\cdots\right]. \tag{18}$$

The coefficient of the third term, $(W^2/24)$, is the second moment of the nearest-neighbor tight-binding conduction electron density of states. The above set of equations are to be solved for the real and imaginary parts of $\Sigma(\omega)$ as a function of ω. Before presenting the numerical solution, we shall examine a number of limits in which analytic results can be found.

It is seen that the above equation has the solution

$$\Sigma(\omega)=\tilde{E}_f \tag{19}$$

in the limit of vanishing impurity concentrations $c\to 0$, or equivalently

$$\Sigma(\omega)=\tilde{E}_f+\Delta E_f \tag{20}$$

when $c\to 1$. Thus, the CPA is exact in the extreme dilute limit.

In the limit $\tilde{V}\equiv 0$, one finds that the solution for $\Sigma(\omega)$ reduces to

$$\Sigma(\omega)=\frac{\omega(E_f+c\Delta E_f)-E_f(E_f+\Delta E_f)}{\omega-E_f-(1-c)\Delta E_f}, \tag{21}$$

which reproduces the exact configurational averaged atomic limit Green's function

$$\tilde{G}^{ff}(\omega)=\frac{1}{\omega-\Sigma(\omega)}=\frac{(1-c)}{\omega-E_f}+\frac{c}{\omega-(E_f+\Delta E_f)}. \tag{22}$$

For $\Delta E_f\to\infty$ and finite but small concentrations, one finds that there is a region where $\tilde{G}^{ff}(\omega)$ is approximately linear in $\omega-\Sigma(\omega)$:

$$\mathrm{Re}\ \tilde{G}^{ff}(\omega)\sim\frac{Z}{W^2}[\Sigma(\omega)-\omega], \tag{23}$$

where Z is a real and large dimensionless coefficient which increases monotonically with decreasing hybridization [$Z\approx 1/24(W/\tilde{V})^4$]. This type of behavior of the local Green's function is already seen in the undoped system, shown in Fig. 2. In this region, the CPA self-energy is given by the approximate expression

$$\Sigma(\omega)\approx\left(\frac{\tilde{E}_f+\omega}{2}\right)\mp\sqrt{\left(\frac{\tilde{E}_f-\omega}{2}\right)^2-\frac{cW^2}{Z}}. \tag{24}$$

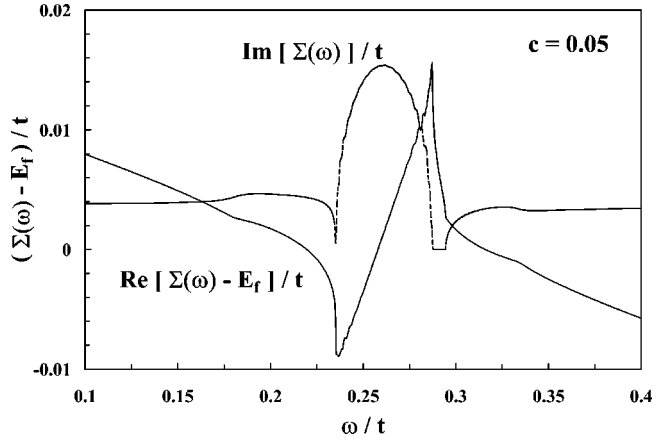

FIG. 3. The ω variation of the CPA self-energy $\Sigma(\omega)$. The real and imaginary parts of $[\Sigma(\omega)-\tilde{E}_f]/t$ are plotted vs ω/t, where t is the tight-binding hopping matrix element. The self-energy was calculated with the same renormalized parameters as in Fig. 1. The real part of the self-energy is shown as a solid line and the imaginary part by the dotted line.

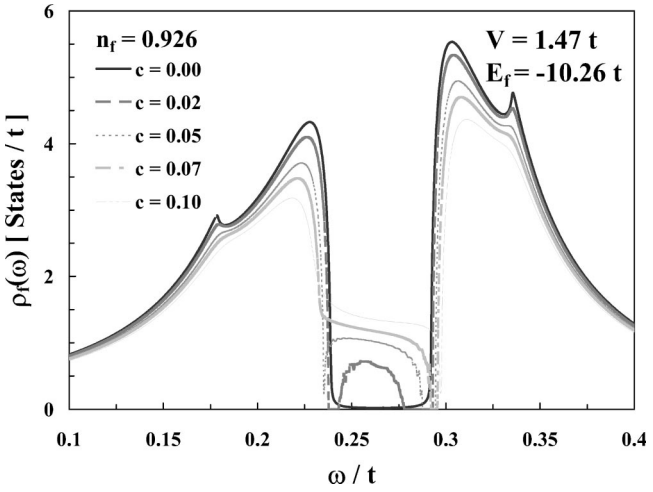

FIG. 4. The f quasiparticle density of states $\rho_f(\omega)$ as a function of ω for various impurity concentrations c. The bare parameters were chosen to be $V=1.47t$ and $E_f=-10.26t$, which correspond to a strong renormalization of the hybridization gap. These parameters correspond to the same values of the renormalized parameters of Fig. 1 and $n_f=0.962$ for zero concentration of impurities. The case corresponding to $c=0$ is shown in (a). The quasiparticle density of states for the doped system are shown in (b), (c), (d), and (e), respectively, for concentrations for $c=0.02$, $c=0.05$, $c=0.07$, and $c=0.10$. As the concentration increases, an impurity band develops in the hybridization gap, and eventually completely fills the gap.

Thus, the density of states within the hybridization gap is zero, except within a small region of width

$$W\sqrt{\frac{4c}{Z}}>|\omega-\tilde{E}_f|, \tag{25}$$

which is controlled by the square root of the concentration. This is in agreement with the findings of previous investigations[29–31] although different approximation schemes were used. In this region there is a nonzero f quasiparticle density of states originating from the impurity-band inside the hybridization gap. The f quasiparticle impurity band density of states has the approximate semielliptical form,

$$\rho_f(\omega)\approx\frac{\sqrt{Zc}}{\pi W}\sqrt{1-\left(\sqrt{\frac{Z}{c}}\frac{(\tilde{E}_f-\omega)}{2W}\right)^2} \tag{26}$$

Hence, the quasiparticle density of states of the impurity-band evaluated at the renormalized f level energy, $\rho_f(\tilde{E}_f)$, is proportional to $c^{1/2}$ and has an integrated weight equal to c.

Inside the f quasiparticle band, away from the gap edges, $|\omega-\tilde{E}_f|\gg|\tilde{V}|^2/W$, the CPA equations can be solved for small concentrations. In this regime, the self-energy is given by

$$\Sigma(\omega)\approx\frac{1}{1-c}[\tilde{E}_f-c\omega\pm ic\pi|\tilde{V}|^2\rho_d^0(\omega)], \tag{27}$$

where $\rho_d^0(\omega)$ is the bare (unhybridized) conduction-band density of states:

$$\rho_d^0(\omega)=\frac{1}{N}\sum_{\underline{k}}\delta(\omega-\epsilon(\underline{k})). \tag{28}$$

A typical form of the exact solution for $\Sigma(\omega)$ is shown in Fig. 3. It is seen that for large frequencies, the real part of the self-energy depends approximately linearly in ω, with a slope of $c/(1-c)$. In this region, the imaginary part of the self-energy is finite and small, in agreement with the approximate result given by Eq. (27). The linear dependence of the real part has the effect of reducing the weight of the quasiparticle bands far from $\tilde{E}_f$ by an amount proportional to c. The real part of the self-energy varies rapidly close to the band edges which has the effect of removing states from this energy region. These states reappear as the impurity band, which is found in an energy range inside the gap where the imaginary part of the self-energy peaks up.

The exact solution for the CPA density of states is shown in Figs. 4 and 5 for various values of the impurity concentration. In Fig. 4(a) the f quasiparticle density of states is shown for the pure system, corresponding to the values of the bare parameters $E_f=-10.26t$ and $V=1.47t$. This set of bare parameters corresponds to the renormalized parameter set $\tilde{E}_f=0.266t$ and $\tilde{V}=0.4t$ and an n_f value of 0.926. The density of states shows the (indirect) hybridization gap located around $\tilde{E}_f$. The asymmetry of the f quasiparticle band density of states about $\tilde{E}_f$ is a consequence of the deviation of n_f from unity and, hence, is a direct manifestation of the mixed valence character of these materials. This can be seen by direct comparison of Fig. 4(a) with Fig. 5(a). The latter is calculated for the bare parameter set $E_f=-5.76t$ and $V=1.22t$ which corresponds to a mixed-valent value of n_f, namely, $n_f=0.831$. The f quasiparticle density of states peaks at energies close to the edges of the hybridization gap. Van Hove singularities are seen at energies deeper inside the f bands. For small values of the concentration $c<0.05$, the impurity band is centered on $\tilde{E}_f$ and is completely contained within the hybridization gap. However, for concentrations c

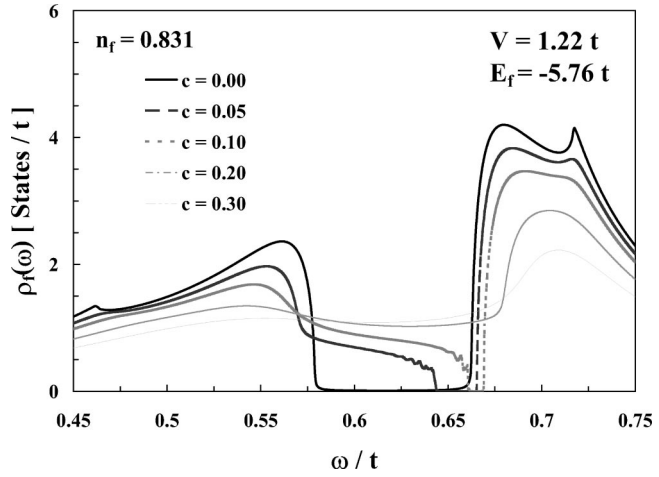

FIG. 5. The f density of states as a function of ω for various impurity concentrations c, in the mixed-valent regime. The values of the unrenormalized parameters used are $V=1.22t$ and $E_f=-5.76t$. This parameters set corresponds to an f occupation number of $n_f=0.831$ for the undoped system. The quasiparticle density of states for the pure system, $c=0$, is shown in (a), while the quasiparticle density of states for $c=0.05$, $c=0.1$, $c=0.2$, and $c=0.3$, respectively, are shown in (b), (c), (d), and (e).

greater than 0.07, the impurity band spans the entire hybridization gap, although a sharp depression occurs just above the range of energies corresponding to the gap even when $c=0.10$. The growth of the impurity band is accompanied by a depletion of the density of states from above and below the hybridization gap edges. The gap width shows only a very slight increase and the depletion mainly comes from a reduction of the heights of the peaks. However, the peak structures at the edges of the f quasiparticle density of states remain quite prominent until it obtains quite large impurity concentrations. By contrast, the Van Hove singularities are rapidly smeared out with increasing impurity concentration.

IV. DYNAMIC RESPONSE

The optical-absorption spectrum is given by the real part of the frequency dependent conductivity tensor $\sigma^{i,j}(\omega)$. The real part of the conductivity is evaluated as

$$\mathrm{Re}[\sigma^{i,j}(\omega)]=\frac{2e^2}{Na^3}\sum_{\underline{k}} v^i(\underline{k})v^j(\underline{k})\int_{-\infty}^{\infty}\frac{dz}{\pi^2}\mathrm{Im}[G^{dd}(\underline{k},z)] \times \mathrm{Im}[G^{dd}(\underline{k},z+\omega)]\left[\frac{f(z)-f(z+\omega)}{\omega}\right], \tag{29}$$

where $v^i(\underline{k})$ is the jth component of the velocity of a conduction electron with Bloch wave-vector $\underline{k}$. The summation over the Bloch wave vector $\underline{k}$ is transformed into the integral over the bare conduction-band density of states weighted with the components of the velocities $v^i(\underline{k})$,

$$\Phi^{i,j}(\epsilon)=\frac{1}{Na^3}\sum_{\underline{k}} v^i(\underline{k})v^j(\underline{k})\,\delta(\epsilon-\epsilon(k)) =\frac{\delta^{i,j}}{a^3}\left(\frac{2ta}{\hbar}\right)^2\int_0^{\infty}\frac{ds}{\pi}\left[\frac{J_0(2ts)^2J_1(2ts)}{2ts}\right]\cos(s\epsilon), \tag{30}$$

where $J_0(x)$ and $J_1(x)$ are Bessel functions. Due to the presence of the Kronecker δ function, the conductivity tensor is diagonal and isotropic. The real part of the conductivity can then be written as

$$\mathrm{Re}[\sigma^{i,j}(\omega)]=2e^2\int_{-\infty}^{\infty}dz\left[\frac{f(z)-f(z+\omega)}{\omega}\right] \times\int_{-\infty}^{\infty}d\epsilon\,\Phi^{i,j}(\epsilon)A_d(\epsilon,z)A_d(\epsilon,z+\omega), \tag{31}$$

where the conduction electron spectral density $A_d(\epsilon,z)$ is given by

$$A_d(\epsilon,z)=\frac{\frac{1}{\pi}\,\mathrm{Im}\,\Sigma(z)\tilde{V}^2}{\{(z-\epsilon)[z-\mathrm{Re}\,\Sigma(z)]-\tilde{V}^2\}^2+[(z-\epsilon)\mathrm{Im}\,\Sigma(z)]^2}. \tag{32}$$

In the limit $c\to 0$, the self-energy is purely real and equal to $\tilde{E}_f$. In this limit, the spectral density is equal to the weighted sum of two δ functions and the ac conductivity reduces to the previously obtained expression:[23]

$$\mathrm{Re}[\sigma^{i,j}(\omega)]=\frac{2e^2\tilde{V}^2}{\omega^2\sqrt{\omega^2-4\tilde{V}^2}}\sum_{\pm}\Phi^{i,j}(\tilde{E}_f\pm\sqrt{\omega^2-4\tilde{V}^2}) \times\left[f\left(\tilde{E}_f-\frac{\omega}{2}\pm\sqrt{\frac{\omega^2}{4}-\tilde{V}^2}\right) -f\left(\tilde{E}_f+\frac{\omega}{2}\pm\sqrt{\frac{\omega^2}{4}-\tilde{V}^2}\right)\right] \tag{33}$$

for $\omega>2\tilde{V}$, and zero if $2\tilde{V}>\omega>0$. The square-root singularity occurs at the threshold energy $\omega=2\tilde{V}$ which corresponds to the direct gap. However, for the pure system electron-electron interactions broaden the singularity into an asymmetric peak. Furthermore, the interactions also result in large $\underline{q}$ fluctuations which assist the electrons in the photon absorption transitions. These fluctuation assisted transitions result in a long tail to the spectra which extends down to a threshold equal to the indirect gap energy.[36,40] For finite impurity concentrations, the impurity scattering is the dominant scattering mechanism and the conductivity has a similar form to that found by including higher-order electron-electron interaction processes. However, while the conductivity of the pure system falls to zero below the indirect gap, the conductivity of the doped system is finite and small below the indirect gap where the conductivity shows a pro-

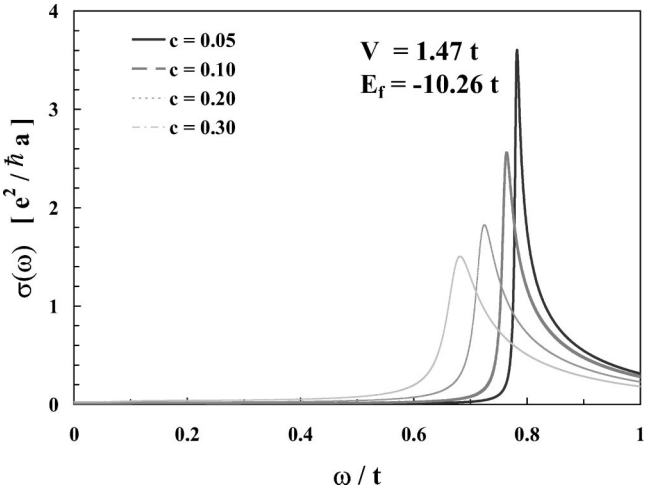

FIG. 6. The diagonal component of the frequency-dependent conductivity, at zero temperature, in units of $e^2/\hbar a$ vs the dimensionless frequency ω/t. For $c=0$ the conductivity has a square-root singularity at the threshold energy $\omega=2\tilde{V}$, which corresponds to the direct gap. For finite concentrations of impurities, the singularity is broadened into a peak which acquires a long tail that stretches down towards zero frequency. The parameters used are the same as in Fig. 4, and the frequency-dependent conductivity is shown in (a), (b), (c), and (d), respectively, for the concentrations $c=0.05$, $c=0.10$, $c=0.20$, and $c=0.30$.

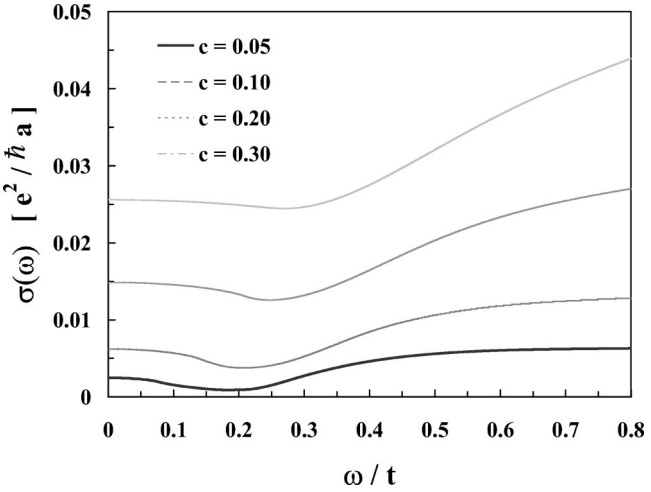

FIG. 7. The diagonal component of the frequency-dependent conductivity for $V=2.686t$ and $E_f=-20.38t$, for the concentrations $c=0.05$, $c=0.10$, $c=0.20$, and $c=0.30$. This parameter set corresponds to a valence of $n_f=0.8614$. In addition to the peak at the direct gap, the tail has a threshold at the indirect gap, below which a small Drude peak due to impurity-band conduction can be observed.

nounced minimum. The small but finite value of the conductivity at $\omega=0$ is due to impurity band conduction. The small magnitude of the $T=0$ Drude peak is caused by the absence of thermally activated conduction processes, which limits the conduction processes to states in the impurity band that are almost localized, that is, the states in the impurity band have a large scattering rate and have low mean-squared velocities. The small magnitude of the mean-square velocity occurs as the impurity band states are mainly formed from the flat portions of the hybridized bands of the pure system near $\tilde{E}_f$. These states not only have a low fraction of conduction band character, but also have $\underline{k}$ values which are close to the top or bottom of the conduction-band and hence, have small magnitudes of $\underline{v}(k)=(1/\hbar[\partial\epsilon(\underline{k})/\partial\underline{k}]$. The frequency dependent conductivity is plotted in Fig. 6 for various impurity concentrations, and $T=0$. The concentration dependence is similar to that found by Okamura *et al.* in experiments on $Yb_{1-x}Lu_xB_{12}$,[27] where the peak was found to broaden and move to lower energies with increasing impurity concentration. Similar results have been found theoretically by Mutou,[44] using the same model as in this work and the disorder was also treated within the CPA However, in Mutou's work the many-body effects were treated, Fig. 7, within the dynamical mean-field approximation which neglects the effect of antiferromagnetic correlations. At finite temperatures, the spectrum shows a thermally activated Drude tail[36] which is dominated by the impurity band states.[30] In accordance with dc transport measurements on $(Ce_{1-x}La_x)_3Bi_4Pt_3$ (Ref. 25) and SmB_6 (Ref. 33) the calculated resistivity shown in Fig. 8 has an exponentially activated regime which goes through a maximum, and then shows a metalliclike temperature variation at the lowest temperatures. The minimum in the resistivity at $T=0$ is due to the energy dependence of the scattering rate, which decreases for states away from the center of the impurity band, as shown in Fig. 2. However, the calculated resistivity differs qualitatively from the experimentally determined resistivity at high temperatures where measurements show that the resistivity is roughly independent of the impurity concentration. This discrepancy is caused by the neglect of intrinsic inelastic-scattering processes which, at high temperatures, should dominate over the elastic impurity scattering rate.

The dynamic magnetic spin-flip response is given by the ronton-pase-approximation-like expression

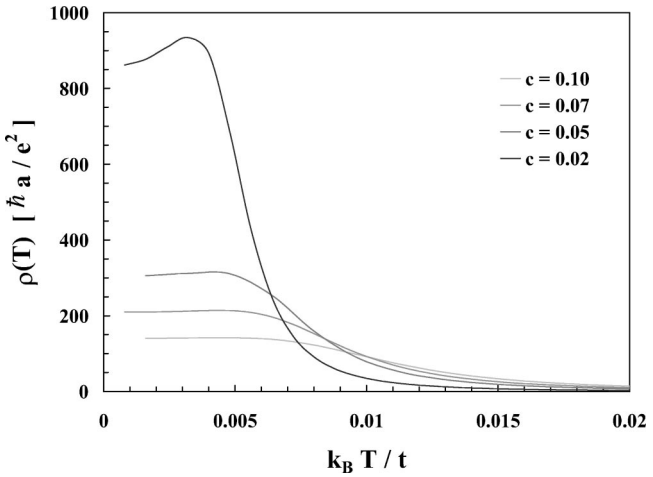

FIG. 8. The temperature dependence of the electrical resistivity $\rho(T)$ for various impurity concentrations. For temperatures of the order of the indirect gap, the resistivity is thermally activated. However, for finite concentrations the resistivity exhibits a maximum at low-temperatures and exhibits a minimum at $T=0$. The parameters used are the same as in Fig. 4.

$$\chi^{+-}(\underline{q},\omega)=g^2\mu_B^2\frac{\chi_0^{+-}(\underline{q},\omega)}{1-J(\underline{q})\chi_0^{+-}(\underline{q},\omega)}. \tag{34}$$

where $\chi_0^{+-}(\underline{q},\omega)$ is the reduced noninteracting quasiparticle susceptibility and $J(\underline{q})$ is the exchange interaction. The reduced susceptibility $\chi_0^{+-}(\underline{q},\omega)$ is given by

$$\mathrm{Im}[\chi_0^{+-}(\underline{q},\omega)]=\frac{1}{N}\sum_{\underline{k}}\pi\int_{-\infty}^{\infty}dz[f(z)-f(z+\omega)] \times A_f(\epsilon(\underline{k}),z)A_f(\epsilon(\underline{k}+\underline{q}),z+\omega). \tag{35}$$

In this expression the f spectral density $A_f(\epsilon,z)$ is given by

$$A_f(\epsilon,z)=\frac{1}{\pi}\frac{(z-\epsilon)^2\mathrm{Im}\,\Sigma(z)}{\{(z-\epsilon)[z-\mathrm{Re}\,\Sigma(z)]-\tilde{V}^2\}^2+[(z-\epsilon)\mathrm{Im}\,\Sigma(z)]^2}. \tag{36}$$

The exchange interaction is calculated as the zero frequency limit:

$$J(\underline{q})=\lim_{\omega\to 0}\frac{1}{N}\sum_{\underline{k}}\left(\frac{|V|^2}{E_f}\right)^2\oint_C\frac{dz}{2\pi i}f(z)G^{dd}(\underline{k},z) \times G^{dd}(\underline{k}+\underline{q},z+\omega), \tag{37}$$

where the contour C encloses all the poles of the Fermi function $f(z)$. For the stoichiometric system, this reduces to the expression[45,46]

$$J(\underline{q})=\frac{1}{N}\sum_{\underline{k}}\left(\frac{|V|^2}{E_f}\right)^2\left(\frac{f^+(\underline{k}+\underline{q})-f^-(\underline{k})}{E^-(\underline{k})-E^+(\underline{k}+\underline{q})}\right) \times|B^+(\underline{k}+\underline{q})|^2|B^-(\underline{k})|^2, \tag{38}$$

where $B^+(\underline{k})$ and $B^-(k)$ are, respectively, the fractional conduction electron character of the wave function of the state with Bloch wave-vector $\underline{k}$ in the upper $(+)$ and lower $(-)$ hybridized bands. This exchange interaction is similar to the Ruderman-Kittel-Kasuya-Yosida interaction but, since the system is gapped, all the processes contributing to the magnetic exchange interaction are virtual processes. The virtual interaction proceeds by the moment on the f ion polarizing the conduction electrons as a result of the Schrieffer-Wolf exchange interaction of strength $|V|^2/E_f$. The conduction electrons transmit the polarization to a second site where it interacts with the local moment via the Schrieffer-Wolf interaction. Due the presence of the conduction electron susceptibility, and as the conduction band is almost half filled, the intersite exchange interaction has a strong antiferromagnetic character.

Inelastic neutron-scattering experiments on CeNiSn (Ref. 47) have been interpreted as showing that the intersite exchange interactions are relatively weak. A possible cause for the relatively weak intersite exchange interaction in the Ce Kondo semiconductors is given by photoemission experiments where the bare f level is found to be about 2–3 eV below the chemical potential. The large value of E_f in the denominator of the Schrieffer-Wolf exchange and could result in a relatively weak intersite interaction. However, a proper description of the inter-site exchange exchange interaction incorporating the Kondo effect[48] is still lacking, and is an area for further research. As a consequence of the weak exchange, the spin exciton is not expected to be fully formed for Ce systems and the main effect of the doping is through the noninteracting quasi-particle susceptibility. The susceptibility is largest for wave vectors near the corner of the Brillouin zone, $\underline{Q}=(\pi/a)(1,1,1)$. This is shown in Fig. 9. The stoichiometric system shows a threshold corresponding to excitations over the indirect gap with a large peak just above the threshold energy. The introduction of impurities reduces the overall intensity of the inelastic peak, and produces a shoulder below the threshold which has an integrated intensity that roughly scales with the impurity concentration for small c. The impurities also produce a quasielastic component to the spectra. The combined effect of the growing quasielastic component and the widening of the shoulder is that of progressively filling the gap in the spectra, as the impurity concentration is increased. The spectra at the zone center is much less intense, as shown in Fig. 10. The zone center spectrum for the stoichiometric system is dominated by a peak at the direct gap, and has a form similar to the optical conductivity. For $q=0$, the introduction of small amounts of impurities produces an inelastic contribution which peaks in the vicinity of the indirect gap. More precisely, the position of the peak correlates with the peak energy of the shoulder in the $q=Q$ spectrum. The magnitude of this peak is much larger than the corresponding tail in the optical conductivity, since the conduction-band character of the states in the vicinity of the gap is suppressed by a factor of order of $|V/t|^2$ and the conduction states which are admixed have velocities close to zero. It is seen that the impurities reduce the propensity for antiferromagnetic correlations and concomitantly increase the propensity for ferromagnetic

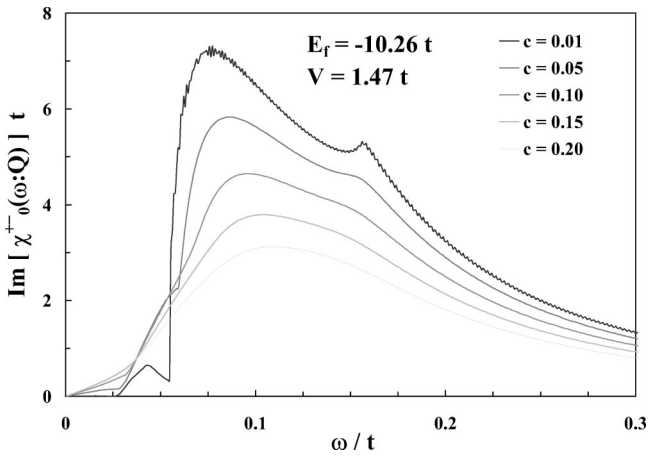

FIG. 9. The imaginary part of the spin-flip component of the frequency-dependent susceptibility tensor $\chi^{+-}(\underline{Q},\omega)$ at the corner of the Brillouin zone and zero temperature for various impurity concentrations. The parameters used are the same as in Fig. 4.

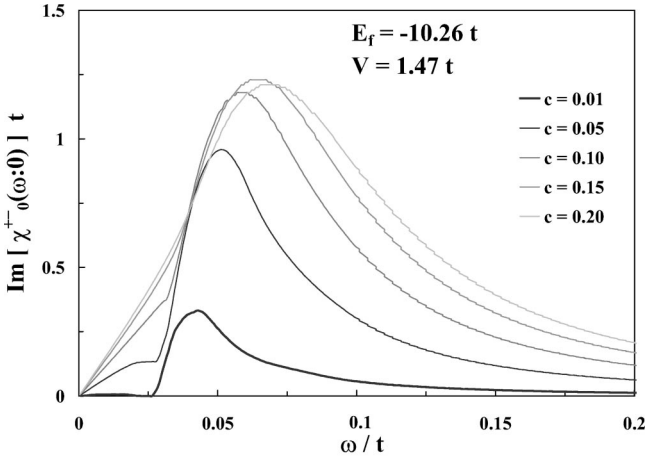

FIG. 10. The imaginary of the spin-flip component of the frequency-dependent susceptibility tensor $\chi^{+-}(\underline{0},\omega)$ at the zone center and zero temperature for various impurity concentrations. The values of the parameters are the same as those given in Fig. 4.

correlations. This observation is qualitatively consistent with the experiments on doped $(Ce_{1-x}La_x)_3Bi_4Pt_3$ where the magnitude of the wave-vector averaged response decreases[49] while the $q=0$ susceptibility grows by 25–35% on increasing x from zero to $x=0.07$.[3] However, even for the largest concentrations, the calculations show that the wave-vector averaged response is still dominated by the antiferromagnetic response. Similar trends to those shown in Fig. 9 were found in the inelastic neutron-scattering spectra from polycrystalline $(Ce_{1-x}La_x)_3Bi_4Pt_3$ measured by Severing *et al.*[49]

By contrast in Yb systems, which are generally more mixed valent than the Ce systems, the bare f level is expected to lie just above the chemical potential and, as a result, the local magnetic moments are expected to be coupled via a strong Heisenberg antiferromagnetic exchange interaction. A sufficiently strong magnetic exchange is expected to result in the formation of a spin exciton which lies within the gap. The spin exciton should show a maximum binding energy at the antiferromagnetic zone boundary, as found in SmB_6.[7] For values of the exchange interaction $J(Q)$ smaller than the critical value, the peak in the spectral density just above the threshold should be enhanced. The theoretical results for the zone corner susceptibility with finite impurity concentrations are shown in Figs. 11(a) and 11(b) for values of $J(Q)$, respectively, above and below the critical value. The values of the bare parameters are $V=2.686t$, $E_f=-20.3826t$, which correspond to an f occupation number of $n_f=0.8614$ and the renormalized parameters $\tilde{V}=1.0t$, and $\tilde{E}_f=0.5833t$. The spectral density of $q=\underline{Q}$ magnetic excitations of the stoichiometric system should show spin-exciton excitations as a sharp Gaussian line within the gap. Since the introduction of impurities produces a shoulder to the gap, the almost singular peak in the real part of the reduced noninteracting quasiparticle susceptibility at the threshold is gradually smeared out with increasing impurity concentration. For systems where the spin exciton is fully developed, introduction of impurities results in a broadening and decrease in the binding energy of the spin exciton, eventually causing the in-gap

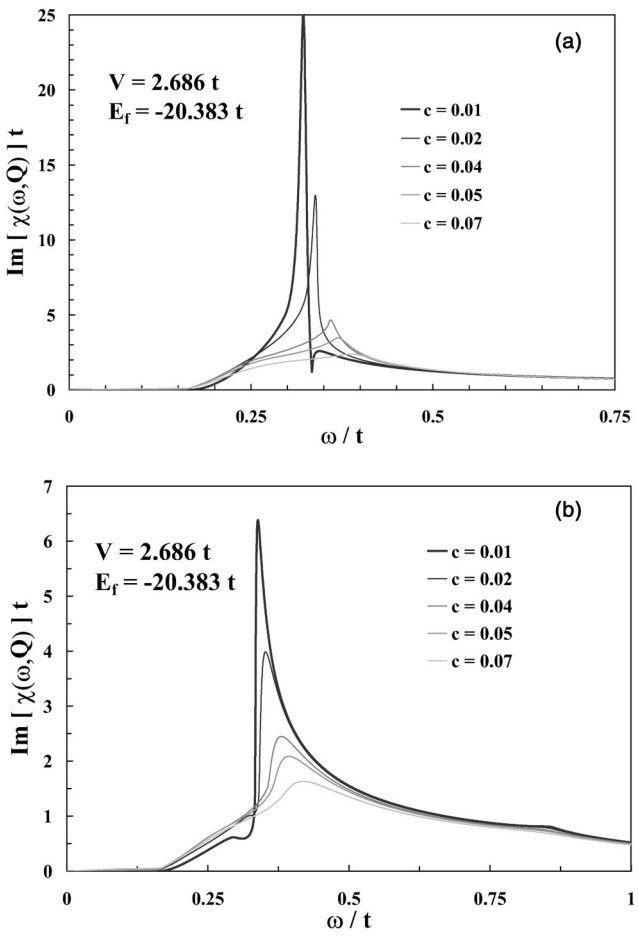

FIG. 11. The inelastic neutron-scattering spectra, at the corner of the Brillouin zone, for various impurity concentrations. In (a) the spectra are shown for a value of $J(Q)=0.7t$ which is greater than that the critical value needed to separate the spin-exciton spectrum from the continuum. The spectrum shows the spin-exciton feature within the indirect gap. The effect of increasing impurity concentrations is that of broadening the spin-exciton peak and lowering its binding energy. For large enough impurity concentrations, the spin-exciton only exists as a virtually bound state. The spectra shown in (b) are calculated for a value of $J(Q)=0.45t$ which is just below the critical value. The continuum spectra are resonantly enhanced near the indirect gap energy. Introduction of impurities rapidly decrease the enhancement of the peak near the threshold.

feature to collapse into the continuum. However, for systems where the interaction is just below the critical value, the stoichiometric system should show a peak above threshold which is enhanced by the magnetic exchange interaction. The enhancement of the peak at the threshold is rapidly washed out with increasing impurity concentrations. The rate at which the intensity of the peak height is reduced with impurity concentrations is strongly dependent on the magnitude of the enhancement. Although the height of the resonance is rapidly decreased by impurities, the magnetic intensity in the gap region is not changed substantially.

Recently, high-resolution inelastic neutron-scattering experiments have been performed on polycrystalline $Yb_{1-x}Lu_xB_{12}$ with $x=0$ and $x=0.25$ (Ref. 37) and $x=0.9$.

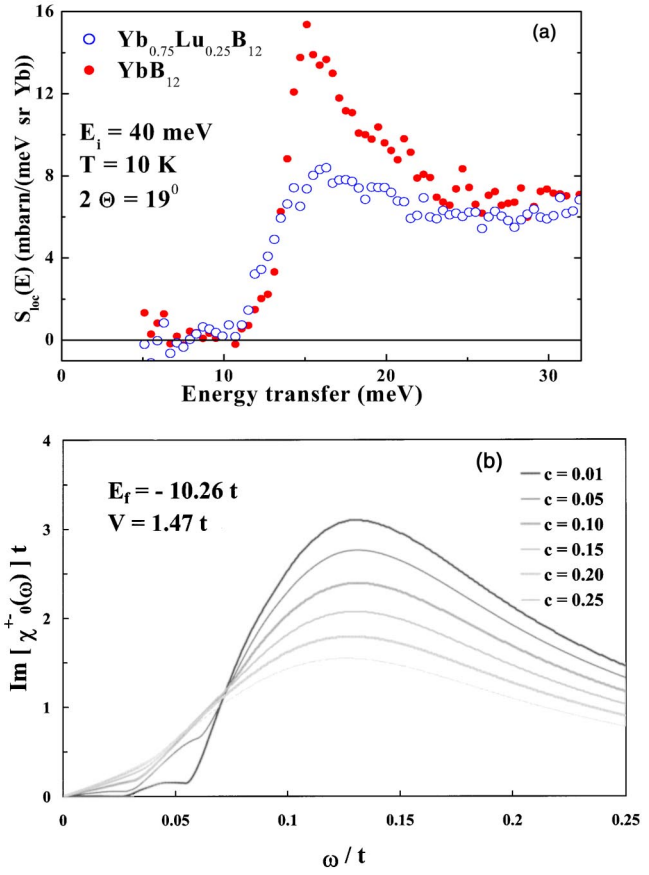

FIG. 12. The magnetic excitation spectra are shown in (a) for $Yb_{0.75}Lu_{0.25}B_{12}$ (open circles) and YbB_{12} (solid circles), measured at $T=10$ K. The data are taken from Ref. 54 The form factor dependence of the data was divided out. The $T=0$ limit of the scattering function may be compared with the calculated imaginary part of the local susceptibility, shown in (b).

The magnitude of the momentum transfer q was sufficiently large, such that the spectrum is representative of an average over the entire Brillouin zone. Thus, the experimental results may be compared with the imaginary part of the local susceptibility. The $x=0$ spectra shows a large asymmetric peak at 15 meV just above the threshold of magnetic excitations, and two other peaks at 23 and 40 meV. For $x=0.25$, the peak at threshold has its intensity reduced by a factor of 2, and there is only a slight change in the spectral density at the threshold energy [see Fig. 12(a)]. Experiments on a sample with $x=0.9$ show that the peaks at 15 and 20 meV are completely suppressed, while the peak at 40 meV retains its form. The peaks at 15 and 20 meV were assigned as being coherent in nature, while the peak at 40 meV was assigned incoherent or single-ion character. The reduction of the intensity of the 15 meV peak by a factor of ≈ 1.9 for an impurity concentration of 25% is inconsistent with the local susceptibility inferred from the single impurity Anderson model, as this should scale directly with the number of Yb atoms. However, the experimentally determined reduction is consistent with the calculated local susceptibility in the absence of a magnetic exchange interaction, shown in Fig. 12(b), and indicates the nonlocal nature of the magnetic fluctuations. The experimentally determined peak is more asymmetric than the calculated spectra and falls off more rapidly near the gap. This has the effect that the present calculations exhibit a larger increase in the spectral intensity in the gap region than seen in the experiments on doped YbB_{12}. The theory implies that the indirect gap of the stoichiometric material is slightly smaller than 13 meV, and that a truly bound spin exciton is not formed. However, the large asymmetry of the experimentally determined peak is consistent with a substantial amount of exchange enhancement and the formation of a virtually bound spin exciton. Further high-resolution inelastic neutron-scattering experiments on single crystals appear to be necessary to establish the q dependence of the spectral peak and to definitively answer the question as to whether a spin exciton exists in YbB_{12}.

Substitutional impurities have been introduced in the semimetal CeNiSn, the properties which have been observed are qualitatively similar to those described in this paper.[50,51] This might have been anticipated, since the Kondo semimetal CeNiSn has been described by a model,[38] which is quite similar to the model used for the Kondo semiconductors.[22] On the other hand, the presence of the anisotropic hybridization gap might result in significant differences with the model considered here, and is a subject that requires further investigation.

V. SUMMARY

The properties of Kondo semiconductors can be described by the Anderson lattice model, close to half filling. The system has an indirect gap between the upper and lower hybridized bands. The substitution of non-f impurities on the f sites produces an impurity band within the gap. On increasing the concentration of the substitutional impurities to a few percent, the impurity band spans the entire gap. The electrical resistivity shows an exponential increase, but saturates at low-temperatures to a value which is controlled by the concentration of impurities. In both the model calculation and experimental measurements,[25,33] the resistivity shows a slight local minimum at $T=0$. The ac conductivity for the pure system is dominated by a peak at the energy of the direct gap. On doping, the peak in the conductivity broadens and develops a tail which extends down to the indirect gap. The peak position is reduced with increasing concentrations, in a manner similar to that found in optical measurements on $Yb_{1-x}Lu_xB_{12}$.[27] At finite concentrations, a small Drude peak appears in the $T=0$ optical conductivity which represents the conduction processes within the almost localized impurity band. We have examined the effect of doping on the magnetic response functions which, since the model is that of an indirect gap semiconductor, behaves markedly different for different momentum transfers. The main effect of doping is that of reducing the antiferromagnetic correlations and increasing the ferromagnetic correlations. This trend is consistent with the observed growth of the static susceptibility with increased doping.[3] It was also found that doping reduces the gap in the wave-vector averaged spectral density and introduces states within the gap, as was seen in inelastic-scattering experiments on $(Ce_{1-x}La_x)_3Bi_4Pt_3$.[49] Recent

high-resolution inelastic neutron-scattering measurements on $Yb_{1-x}La_xB_{12}$ compounds[37] as a function of doping are inconsistent with the magnetic fluctuations being of local character. The results appear to be consistent with either the existence of a virtually bound spin exciton or the enhancement of the peak near threshold due to a strong antiferromagnetic exchange interaction.

Several areas remain ripe for future investigation. These include the theoretical description of the introduction of a low density of either electrons or holes into a Kondo insulator, a situation which is perhaps realized in the compound $YbAl_3$;[52,53] the adiabatic continuation of the model describing the high-energy excitations (with either $J=5/2$ for Ce or $J=7/2$ for Yb) to the effective low-energy doubly degenerate model which describes the semiconductor phase; theoretical studies of the effect of impurities in the anisotropic Kondo semimetals, such as CeNiSn; and finally, a rigorous theoretical description of intersite interactions incorporating the Kondo effect.

ACKNOWLEDGMENTS

This work was funded by the U.S. Department of Energy, Office of Basic Energy Sciences through Grant No. DEFG02 01ER45872. The author would like to thank Dr. P. A. Alekseev and Dr. J.-M. Mignot for sharing their unpublished data and stimulating this work. The author would also like to thank Dr. J. C. Cooley, or Z. Fisk, Dr. S. R. Horn, C.-L. Lin, Dr. H. Okamura, Dr. J.W. Rasul, Dr. P. Schlottmann, Dr. S. Suga, Dr. T. Takabatake, and Dr. J. D. Thompson for enlightening discussions on this topic. I would also like to thank Professor Raza Tahir-Kheli for several discussions on various aspects of the CPA

[1] G. Aeppli and Z. Fisk, Comments Condens. Matter Phys. **16**, 155 (1992).
[2] P.S. Riseborough, Adv. Phys. **49**, 257 (2000).
[3] M.F. Hundley, P.C. Canfield, J.D. Thompson, Z. Fisk, and J.M. Lawrence, Phys. Rev. B **42**, 6842 (1990).
[4] T. Kasuya, K. Takegahara, T. Fujita, and E. Banai, J. Phys. Colloq. **5**, 308 (1979).
[5] M. Kasaya, F. Iga, K. Negishi, S. Nakai, and T. Kasuya, J. Magn. Magn. Mater. **31-34**, 437 (1983).
[6] A. Severing, J.D. Thompson, P.C. Canfield, Z. Fisk, and P.S. Riseborough, Phys. Rev. B **44**, 6832 (1991).
[7] P.A. Alekseev, J.-M. Mignot, J.M. Rossat-Mignod, V.N. Lazukov, and I.P. Sadikov, Physica B **186-188**, 384 (1993); P.A. Alekseev, J.-M. Mignot, J.M. Rossat-Mignod, V.N. Lazukov, I.P. Sadikov, E.S. Konvalova, and Yu.B. Paderno, J. Phys.: Condens. Matter **7**, 289 (1995).
[8] A. Bouvet, T. Kasuya, M. Bonnet, L.P. Regnault, J.M. Rossat-Mignod, F. Iga, B. Fak, and A. Severing, J. Phys.: Condens. Matter **10**, 5667 (1998).
[9] E.V. Nefeodova, P.A. Alekseev, J.-M. Mignot, V.N. Lazukov, I.P. Sadikov, Yu.B. Paderno, N. Yu Shitsevalova, and R.S. Eccleston, Phys. Rev. B **60**, 13 507 (1999); P.A. Alekseev, E.V. Nefeodova, U. Staub, J.-M. Mignot, V.N. Lazukov, I.P. Sadikov, L. Solderholm, S.R. Wassermann, Yu.B. Paderno, N. Yu Shitsevalova, and A.P. Murani, *ibid.* **63**, 064411 (2001).
[10] B. Bucher, Z. Schlesinger, P.C. Canfield, and Z. Fisk, Phys. Rev. Lett. **72**, 522 (1994).
[11] B. Gorshonov, N. Sluchanko, A. Volkov, M. Dressel, G. Knebel, A. Loidl, and S. Kunii, Phys. Rev. B **59**, 1808 (1999).
[12] S. Kimura, T. Nanba, S. Kunii, and T. Kasuya, Phys. Rev. B **50**, 1406 (1994).
[13] H. Okamura, S. Kimura, H. Shinozaki, T. Nanba, F. Iga, N. Shimuzu, and T. Takabatake, Phys. Rev. B **58**, 7496 (1998).
[14] T. Takabatake, Y. Nakazawa, and M. Ishikawa, Jpn. J. Appl. Phys., Suppl. **26**, 547 (1987).
[15] S.K. Malik and D.T. Adroja, Phys. Rev. B **43**, 6277 (1991).
[16] M.B. Hunt, M.A. Chernikov, E. Felder, H.R. Ott, Z. Fisk, and P.C. Canfield, Phys. Rev. B **50**, 14 933 (1994).
[17] K. Izawa, T. Suzuki, T. Fujita, T. Takabatake, G. Nakamaoto, H. Fujii, and K. Maezawa, Phys. Rev. B **59**, 2599 (1999).
[18] T. Terashima, C. Terakura, S. Uji, H. Aoki, Y. Echizen, and T. Takabatake, Phys. Rev. B **66**, 075127 (2002).
[19] C. Fu and S. Doniach, Phys. Rev. B **51**, 17 439 (1995).
[20] Y. Takahashi, J. Phys.: Condens. Matter **10**, L671 (1998).
[21] K. Urasaki and T. Saso, Physica B **281**, 313 (2000).
[22] P.S. Riseborough, Phys. Rev. B **45**, 13 984 (1992).
[23] P.S. Riseborough, Physica B **199-200**, 446 (1994).
[24] M.F. Hundley, J.D. Thompson, P.C. Canfield, and Z. Fisk, Physica B **199-200**, 443 (1994).
[25] M.F. Hundley, P.C. Canfield, J.D. Thompson, and Z. Fisk, Phys. Rev. B **50**, 18 142 (1994).
[26] F. Iga, M. Kasaya, and T. Kasuya, J. Magn. Magn. Mater. **52**, 279 (1985).
[27] H. Okamura, M. Matsunami, T. Inaoka, T. Nanba, S. Kimura, F. Iga, S. Hiura, J. Klijin, and T. Takabatake, Phys. Rev. B **62**, R13265 (2000).
[28] R. Sollie and P. Schlottmann, J. Appl. Phys. **69**, 5478 (1991); **70**, 5803 (1991).
[29] P. Schlottmann, Phys. Rev. B **46**, 998 (1992).
[30] J.W. Rasul, Phys. Rev. B **51**, 2576 (1995); **56**, 13 701 (1997).
[31] Z.-Z. Li, W. Xu, C. Chen, and M.-W. Xiao, Phys. Rev. B **50**, 11332 (1994).
[32] J.W. Allen, B. Batlogg, and P. Wachter, Phys. Rev. B **20**, 4807 (1979).
[33] J.C. Cooley, M.C. Aronson, Z. Fisk, and P.C. Canfield, Phys. Rev. Lett. **74**, 1629 (1995); J.C. Cooley, M.C. Aronson, A.C. Lacerda, Z. Fisk, and P.C. Canfield, Phys. Rev. B **52**, 7322 (1995).
[34] L. Frankowski and P. Wachter, Solid State Commun. **41**, 577 (1982).
[35] S. Kunii, J. Magn. Magn. Mater. **63-64**, 673 (1987).
[36] P.S. Riseborough, Ann. Phys. (Leipzig) **9**, 813 (2000).
[37] P.A. Alekseev, J.-M. Mignot, K.S. Nemovski, R. Kahn, N.Yu. Shitsevalova, R.I. Bewley, R.S. Eccleston, E.S. Clementov, V.N. Lazukov, E.V. Nefeodova, I.P. Sadikov, and N.N. Tiden, Appl. Phys. A: Mater. Sci. Process. **A75**, 1 (2002).
[38] H. Ikeda and K. Miyake, J. Phys. Soc. Jpn. **65**, 1769 (1996).

[39] Y. Kagan, K.A. Kikoin, and A.S. Mishchenko, Phys. Rev. B **55**, 12 348 (1997).
[40] P.S. Riseborough, Phys. Rev. B **58**, 15 534 (1998).
[41] P. Soven, Phys. Rev. **156**, 809 (1967).
[42] B. Velický, S. Kirkpatrick, and H. Ehrenreich, Phys. Rev. **175**, 747 (1968).
[43] R.J. Elliott, J.A. Krumhansl, and P.L. Leath, Rev. Mod. Phys. **46**, 465 (1975).
[44] T. Mutou, Phys. Rev. B **64**, 1651031 (2001).
[45] S. Doniach, Phys. Rev. B **35**, 1814 (1987).
[46] A. Houghton, N. Read, and H. Won, Phys. Rev. B **37**, 3782 (1988).
[47] T. Mason, G. Aeppli, A.P. Ramierez, K.N. Clausen, C. Broholm, N. Stücheli, E. Bucher, and T.T.M. Palstra, Phys. Rev. Lett. **69**, 490 (1992).
[48] S. Doniach, Physica B & C **91**, 231 (1977).
[49] A. Severing, T. Perring, J.D. Thompson, P.C. Canfield, and Z. Fisk, Physica B **199&200**, 480 (1994).
[50] T. Takabatake, Y. Echizen, T. Yoshino, K. Kobayashi, G. Nakamoto, H. Fujii, and M. Sera, Phys. Rev. B **59**, 13 878 (1999).
[51] K. Nakamura, Y. Kitaoka, K. Asayama, and T. Takabatake, Phys. Rev. B **53**, 6385 (1996).
[52] A.P. Murani, Phys. Rev. Lett. **54**, 1444 (1985).
[53] H. Okamura, T. Ebihara, and T. Nanba, *Heavy Quasiparticles and Pseudogap Formation in $YbAl_3$: Optical Conductivity Study*, Special Issue of Acta Phys. Pol. B **34**, 1075 (2003).
[54] P.A. Alekseev, J.-M. Mignot, and R. Bewley, ISIS experimental report RB12 830, 2002 (unpublished).